Improving a Low Axial Resolution Due to Improper Wavelength Calibration in Spectral-Domain Optical Coherence Tomography

Mengsi Zhang, Songjie Luo, Osami Sasaki, Ziyang Chen, and Jixiong Pu

***Abstract*—Inaccurate wavelength calibration for spectral-domain optical coherence tomography (SD-OCT) generates a depth-dependent broadening of coherence peak. In this paper, a simple technique is proposed to eliminate the wavelength calibration error by the spectral-resolved interference signal correction. Utilizing the nonlinear component of phase distribution in wavenumber domain and the optimization algorithm, an optimized coefficient is obtained and used to improve the axial resolution. The simulation was carried out to verify the principle of the proposed method. In experiment, a sample of reflecting mirror was used to obtain the nonlinear phase and the optimized coefficient for correcting the spectral-resolved interference signals of tapes and chicken breast. In the measurement of a layer of tape with a thickness of about 1.5 mm, two full width half maximum (FWHM) of amplitude generated from the front and rear surfaces dropped to 7.73 μm and 9.99 μm from 33.57 μm and 55.36 μm after the signal correction. A self-made sample containing 6 layers of tape and a part of chicken breast were tested, whose sharpness metric grow larger than 12.8% after signal correction. This method provides a simple way to improve the image quality of SD-OCT in improper wavelength calibration.**

***Index Terms*—Image resolution, optical coherence tomography.**

I. Introduction

OPTICAL coherence tomography (OCT) is a noninvasive imaging modality with high-resolution and three-dimension that emerged for biological tissues imaging [1], [2]. Considering the requirement of high-speed and good image contrast, the spectral-domain OCT is well developed compared with the time-domain OCT despite the disadvantage of the complex conjugate ambiguity [3], [4], [5], [6]. In SD-OCT, the optical signal generated by a broadband light is detected by a spectrometer made of diffraction grating, lens and a line-scan camera. Inexact relationship between the pixel of camera and the wavelength induces the nonlinear component for wavenumber which brings the depth-dependent broadening of the coherence peak. Achieving the accurate wavelength value on each pixel is critical to attain images with high axial resolution.

Exact relationship between the pixel and wavelength is implemented by wavelength calibration methods. The standard light source with well-known wavelengths is widely used to determine the wavelengths of some pixels. Then, the polynomial with proper coefficients is fitted to express the relationship between all pixels of camera and corresponding wavelengths [7], [8], [9], [10]. To avoid requirement of additional light sources, the monochromator to filter the broadband spectrum is used as the standard light source flexibly [10]. Moreover, a fringe mapping method is proposed to calibrate wavelength utilizing the interference signal generated by two reflecting mirrors in SD-OCT. Comparing the interference signal detected by the self-made spectrometer and the standard spectrometer, the wavelength distribution is calibrated accurately by analyzing the peaks of the spectral interference fringes of SD-OCT [11], [12]. However, the requirement of additional setup brings inconvenience for the above methods. Other algorithm has been proposed to eliminate the wavelength calibration error by generating a sinusoidal spectral modulation in wavenumber domain [13], [14], [15], [16]. Similar to the dispersion generated by the optics in system, the improper wavelength calibration also brings the nonlinear component for the phase. Thus, the phase information is investigated to calibrate the wavelength distribution [17], [18], [19], [20].

In the manuscript, a signal correction method is proposed to improve the axial resolution of SD-OCT in improper wavelength calibration. Instead of calculating the exact wavelength value of each pixel of spectral analyzer, the nonlinear phase and optimized coefficient obtained from the signals generated by the two reflecting mirrors are applied for the reconstruction of spectral-resolved interference signal of tested samples. A simulation is carried out to verify the principle. The experiment of imaging of tapes and chicken breast is performed to prove the effectiveness of the method. Since the dispersion generated by the optics and samples bring nonlinear phase component for the spectral-resolved interference signal, the proposed method provides a possibility to simultaneously

Manuscript received 3 February 2024; revised 30 April 2024; accepted 8 May 2024. Date of publication 13 May 2024; date of current version 4 July 2024. This work was supported in part by the National Natural Science Foundation of China under Grant 62005086 and in part by the Fundamental Research Funds for the Central Universities under Grant ZQN-1111. *(Corresponding author: Songjie Luo.)*

Mengsi Zhang, Songjie Luo, Osami Sasaki, and Ziyang Chen are with the Fujian Provincial Key Laboratory of Light Propagation and Transformation, College of Information Science and Engineering, Huaqiao University, Xiamen 361021, China (e-mail: zms17396356093@163.com; songjie@hqu.edu.cn; osamija@gmail.com; ziyang@hqu.edu.cn).

Jixiong Pu is with the New Engineering Industry College, Putian University, Fujian 351100, China (e-mail: jixiong@hqu.edu.cn).

Digital Object Identifier 10.1109/JPHOT.2024.3399736

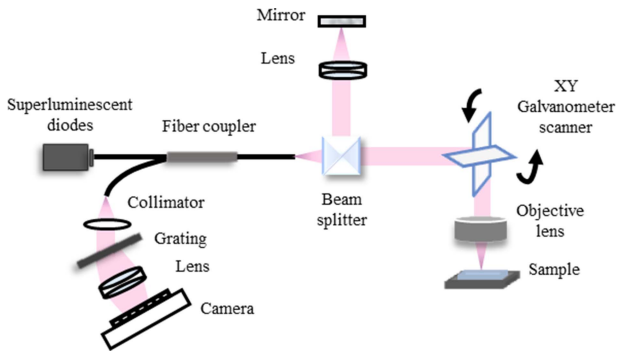

Fig. 1. Diagram of the SD-OCT.

decrease the effect of dispersion and improper wavelength calibration.

II. Theory

Fig. 1 shows the diagram of the commercial SD-OCT. The reflecting mirror is used as a sample to generate the spectral-resolved interference signal. Denoting the path distance as Δz, the spectral-resolved interference signal is given by

$$S(\lambda) = I_0(\lambda) + I_1(\lambda)\cos\left[\frac{4\pi\Delta z}{\lambda}\right] \tag{1}$$

where λ is the wavelength. $I_0(\lambda)$ is spectral intensity of the two beams directly reflected from the reference and sample, and $I_1(\lambda)$ is the visibility function. Normally, wavelength distribution detected by the pixels of camera is expressed as the polynomial [10], [21]:

$$\lambda(n) = c_0 + c_1 n + c_2 n^2 + c_3 n^3 \tag{2}$$

where n is the pixel number and c_0, c_1, c_2, c_3 are typical calibrated coefficients. To simplify the derivation, the spectral-resolved interference signal is denoted as

$$S(\sigma) = I_0(\sigma) + I_1(\sigma)\cos[4\pi\Delta z\sigma] \tag{3}$$

where $\sigma = 1/\lambda$ is the wavenumber. With the improper wavelength calibration, the mismatch between wavelengths and pixels in SD-OCT deviates the coefficient of c_0, c_1, c_2, c_3 in (2) from their actual values. The inexact wavenumber distribution is expressed as the $\sigma+e(\sigma)$, where the $e(\sigma)$ is the wavelength calibration error. Therefore, the spectral-resolved interference signal obtained by SD-OCT with inaccurate wavenumber value is given by

$$S_I(\sigma) = I_0[\sigma + e(\sigma)] + I_1[\sigma + e(\sigma)]\cos\{4\pi\Delta z[\sigma + e(\sigma)]\} \tag{4}$$

The existence of $4\pi\Delta z e(\sigma)$ component in phase distribution brings the broaden of coherence peak with the increase of Δz. Expressing the $e(\sigma)$ as the polynomial of $a_0+a_1\sigma+a_2\sigma^2+a_3\sigma^3+\ldots$, the phase $\varphi_I(\sigma)$ of $S_I(\sigma)$ is given by

$$\begin{aligned}\varphi_I(\sigma) &= 4\pi[\Delta z(\sigma + a_0 + a_1\sigma + a_2\sigma^2 + a_3\sigma^3 + \ldots)] \\ &= 4\pi[\Delta z(\sigma + a_0 + a_1\sigma)] + E(\sigma)\end{aligned} \tag{5}$$

where the $E(\sigma) = 4\pi\Delta z(a_2\sigma^2 + a_3\sigma^3 + \ldots)$ is the nonlinear component of the phase distribution.

The $E(\sigma)$ is acquired by removing the linear component $4\pi\Delta z(\sigma+a_0+a_1\sigma)$ obtained through least square method from the $\varphi_I(\sigma)$. In order to remove the $E(\sigma)$ from $S_I(\sigma)$, the wavenumber value σ of $S_I(\sigma)$ is replaced by $\sigma+CE(\sigma)$, where C is the coefficient. The phase $\varphi_c(\sigma)$ of corrected spectral-resolved interference signal $S_c(\sigma)$ is derived as

$$\begin{aligned}\varphi_c(\sigma) = 4\pi\{&\Delta z[a_0 + (a_1+1)\sigma] + CE(\sigma)\Delta z(a_1+1)\} \\ &+ E[\sigma + CE(\sigma)]\end{aligned} \tag{6}$$

Because the value of C is small, the $E[\sigma+CE(\sigma)]$ in (6) is approximated as $E(\sigma)$. Thus the $\varphi_c(\sigma)$ is given by

$$\varphi_c(\sigma) \approx 4\pi\Delta z[a_0+(a_1+1)\sigma] + E(\sigma)[4\pi C\Delta z(a_1+1)+1] \tag{7}$$

The term of $E(\sigma)[4\pi C\Delta z(a_1+1)+1]$ brings the broaden of amplitude, which is available to be decreased by selecting the proper coefficient C. When the optimized $C = -1/[4\pi\Delta z(a_1+1)]$ is selected, the $\varphi_c(\sigma)$ is derived as

$$\varphi_c(\sigma) = 4\pi\Delta z[a_0 + (a_1+1)\sigma] \tag{8}$$

Since the $\varphi_c(\sigma)$ in (8) will provide the minimum FWHM of amplitude of Fourier transformed $S_c(\sigma)$, the optimized C is found by the its amplitude distribution. In simulation, the calculated value of $C = -1/[4\pi\Delta z(a_1+1)]$ and optimized C determined by the minimum FWHM of amplitude of Fourier transformed $S_c(\sigma)$ will be compared to prove the theory.

Meanwhile, there are two questions must be investigated. Firstly, the $\varphi_c(\sigma)$ in (6)–(8) contains parameters of a_0 and a_1 which will change the position of amplitude of Fourier transformed $S_c(\sigma)$ linearly from actual Δz with the increase of Δz. It is necessary to find the relation between the actual Δz and the calculated Δz from $S_c(\sigma)$, and use that to correct the position of amplitude distribution. Secondly, in the measurement of sample with complex multi-layer structure, such as the biological tissue, the detected spectral-resolved interference signal contains the light reflected from different depths of sample, whose values of Δz are expressed as Δz_1, Δz_2, Δz_3 …. For $S_c(\sigma)$ with the value of Δz_1, the optimized coefficient is $C_1 = -1/[4\pi\Delta z_1(a_1+1)]$. Performing the $C_1 = -1/[4\pi\Delta z_1(a_1+1)]$ on $S_c(\sigma)$ with the value of Δz_2, the term of $E(\sigma)[4\pi C_1\Delta z_2(a_1+1)+1]$ in (7) is not equal to zero anymore. It indicates that only one coefficient of C cannot correct the spectral-resolved interference signals with different Δz perfectly. Thus, it is important to find the optimized coefficient C considering the entire image quality through the algorithm.

An algorithm is used to find the optimized C as shown in Fig. 2. 8 groups of $S_I(\sigma)$ with different OPD are detected by moving positions of the reflecting mirror, which are regarded as the signals reflected from different depths of sample. Nonlinear phase component $E(\sigma)$ is obtained from anyone group of $S_I(\sigma)$. The value σ of 8 $S_I(\sigma)$ is replaced by $\sigma+CE(\sigma)$ to obtain the corrected spectral-resolved interference signal $S_c(\sigma)$. The 8 amplitude distributions of Fourier transformed $S_c(\sigma)$ are used to calculate the standard deviation (STD), whose value varies with the change of C. When the value of STD reaches the minimum,

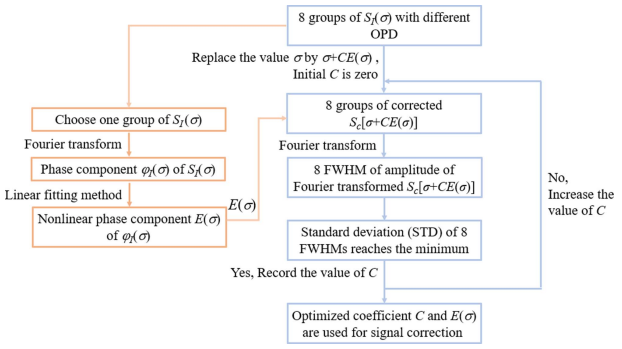

Fig. 2. Flow diagram of algorithm to find the optimized coefficient C.

its value of C is regarded as the optimized coefficient and used to correct any other spectral-resolved interference signal produced by complicated samples with the data of $E(\sigma)$. In order to find the optimized coefficient C with small computational complexity, it is suggested that the STD of 8 FWHMs of amplitude distributions are calculated in the C of $[-10^{-i}, -10^{-i-1}]$ with 100 equal intervals, where the i is the positive integer. In simulation, the values of i are set from 1 to 6, because the STDs remain almost unchanged at i = 6. By changing the values of C in 6 ranges that generated by different values of i, the 6 groups of STD distribution are obtained. The range of C, which owns the minimum STD, is selected to further obtain the accurate minimum STD again. Here, the range of C with i = 3 is selected which has starting value of $C = -10^{-3}$ and ending value of $C = -10^{-4}$. The range of $[-10^{-3}, -10^{-4}]$ is divided to 2000 equally intervals and used to calculated the STD. The optimized coefficient C is determined by the accurate minimum value of STD chosen from the 2000 values. It is flexible to choose the number of intervals in the range of $[-10^{-3}, -10^{-4}]$. Denoting the STDs provided by the adjacent value to optimized coefficient C and the optimized coefficient C as STD_1 and STD_2, any number of intervals is available which provide the $|STD_1 - STD_2|/ STD_2 < 0.01$.

The system dispersion caused by the optics in system is not discussed in the theory part because it is small in the experimental SD-OCT system. When the system dispersion is large, it is necessary to eliminate it before the signal correction. One method had been proposed to extract the system dispersion from two spectral-resolved interference signals detected by sample of reflecting mirror with opposite optical path difference [22]. Here, the similar approach is given to obtain the system dispersion $\varphi_d(\sigma)$. The phase extracted from the spectral-resolved interference signal generated by sample of mirror is expressed as $\varphi_I(\sigma) = \Delta z f(\sigma) + \varphi_d(\sigma)$ according to the (5), where $f(\sigma) = 4\pi(\sigma + a_1\sigma + a_2\sigma^2 + a_3\sigma^3 + \ldots)$. Denoting the phase of two spectral-resolved interference signals with Δz_1 and Δz_2 as $\varphi_{I1}(\sigma)$ and $\varphi_{I2}(\sigma)$, the $f(\sigma)$ is obtained by $[\varphi_{I2}(\sigma) - \varphi_{I1}(\sigma)]/(\Delta z_2 - \Delta z_1)$. Next, the $\varphi_d(\sigma)$ is achieved by subtracting the $\Delta z_1 f(\sigma)$ from the $\varphi_{I1}(\sigma)$, and eliminated from original spectral-resolved interference signal through Hilbert transform [6]. Since 8 groups of spectral-resolved interference signals with a uniform interval of 300 μm are obtained in experiment, any two groups of signals can be chosen to obtain and eliminate the $\varphi_d(\sigma)$.

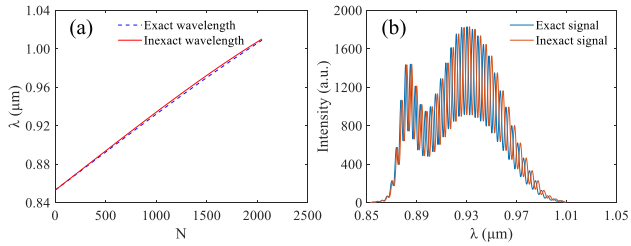

Fig. 3. The spectral-resolved interference signals generated by the exact and inexact wavelength distributions. (a) Wavelength distributions. (b) Spectral-resolved interference signals.

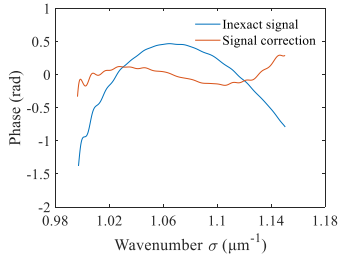

Fig. 4. Nonlinear phase distributions obtained from the spectral-resolved interference signal without and with signal correction using the optimized coefficient C.

III. Simulation

A simulation was carried out to verify the proposed method. Since a commercial SD-OCT was used in experiment, its exact wavelength distribution expressed as $\lambda = c_0 + c_1 n + c_2 n^2 + c_3 n^3$ was carried out to generate the spectral-resolved interference signal, where the $c_0 = 0.8528$, $c_1 = 7.889 \times 10^{-5}$, $c_2 = 1.5235 \times 10^{-9}$, $c_3 = -1.3993 \times 10^{-12}$ and n was the integer from 0 to 2047. Here, other coefficients of $c_0 = 0.8528$, $c_1 = 8.143 \times 10^{-5}$, $c_2 = 1.442 \times 10^{-9}$, $c_3 = -1.808 \times 10^{-12}$ were chosen to simulate the inexact wavelength distribution caused by wavelength calibration error as shown in Fig. 3(a). Fig. 3(b) shows one spectral-resolved interference signal with the exact and inexact wavelength distributions. The inexact wavelength distribution distorts the spectral-resolved interference signal from its real waveform.

The spectral-resolved interference signal with inexact wavelength distribution and $\Delta z = 100$ μm in Fig. 3(b) was chosen to calculate the value of $C = -1/[4\pi\Delta z(a_1+1)]$. The value of $a_1 = 8.78 \times 10^{-3}$ was obtained from the $e(\sigma)$ by linear fitting method, thus the value $C = -7.89 \times 10^{-4}$ was acquired by calculation, which provided the FWHM of 7.31 μm for the amplitude of Fourier transformed $S_c(\sigma)$.

Next, the nonlinear component $E(\sigma)$ of spectral-resolved interference signal with inexact wavelength distribution in Fig. 3(b) was achieved as the shown in Fig. 4 with the magnitude of about 1.8 rad, and used for signal correction. Performing the different value of C on signal correction, the value of $C = -8.38 \times 10^{-4}$ provided the minimum FWHM of 7.17 μm for

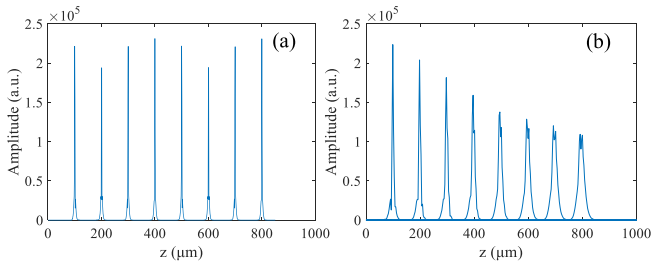

Fig. 5. Amplitude distributions obtained from spectral-resolved interference signals with (a) exact and (b) inexact wavelength distributions.

TABLE I
THE CALCULATED Δz AND SCALE FACTOR VALUES OBTAINED FROM THE SPECTRAL-RESOLVED INTERFERENCE SIGNALS IN SIMULATION

Δz (μm)	100	200	300	400	500	600	700	800
Calculated Δz (μm)	99.00	197.90	297.00	395.94	494.93	594.02	692.94	791.87
R	1.0101	1.0106	1.0101	1.0103	1.0102	1.0101	1.0102	1.0103

the amplitude of Fourier transformed $S_c(\sigma)$. The similar values C of -7.89×10^{-4} and -8.38×10^{-4} and FHWMs of 7.31 μm and 7.17 μm reveal that the optimized value of C determined by minimum FWHM of the amplitude distribution is almost equal to its theoretical value, and the algorithm is available for signal correction. The minor difference is caused by the formula approximation shown in (7). After the signal correction by the $C = -8.38 \times 10^{-4}$, the nonlinear phase component of $S_c(\sigma)$ was obtained in Fig. 4, whose magnitude was about 0.1 rad. It indicates that the nonlinear component of $E(\sigma)$ was significantly reduced.

To display the impact of two groups of wavelength distribution in Fig. 3(a), the 8 spectral-resolved interference signals generated with the interval of 100 μm for Δz were carried out to obtain the amplitude distributions as shown in Fig. 5(a) and (b), respectively. Fig. 5(b) shows that the FWHM of amplitude enlarges with the increase of z, which provide the lower axial resolution compared to Fig. 5(a).

Meanwhile, the peak positions of amplitudes in Fig. 5(b) that differ from the preset values of Δz reveal the parameters of a_0 and a_1 in (6)–(8) brings the position error of measured reflecting surface of sample. Performing the inverse Fourier transform on the Fourier transformed $S_I(\sigma)$, its phase distribution $\varphi_I(\sigma)$ was obtained. The FDA method was carried out to calculate Δz from the $\varphi_I(\sigma)$ shown in Table I [23], where the scale factor between the Δz and calculated Δz was denoted as $R = (\Delta z /$ Calculated $\Delta z)$. It was made clear that the average scale factor between the Δz and calculated Δz was $R = 1.0102$. Thus, the position of amplitude distribution obtained from the spectral-resolved interference signal with inexact wavelength calibration should be multiplied by R to provide the exact position of the reflecting surface of sample.

The nonlinear component of phase distribution $E(\sigma)$ was obtained from anyone group of 8 spectral-resolved interference signals with inexact wavelength distribution. Here, the $E(\sigma)$ in

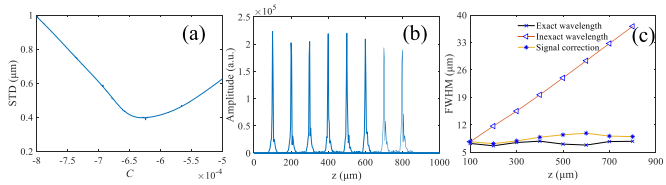

Fig. 6. Signal correction procedure and result. (a) Standard derivations of the FWHM of 8 amplitudes after signal correction with different coefficients C. (b) The amplitude distributions after signal correction with optimized C. (c) FWHM of amplitude distributions obtained with exact wavelength distribution, inexact wavelength distribution and signal correction.

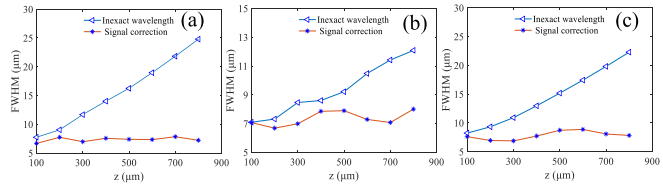

Fig. 7. FWHM of amplitude distributions obtained with inexact coefficient of c_1, c_2 and c_3 in (2) and signal correction. (a) c_1 increases 20% from its exact value. (b) c_2 increases 20% from its exact value. (c) c_3 increases 20% from its exact value.

Fig. 4 obtained from the spectral-resolved interference signal with $\Delta z = 100$ μm was used for signal correction. The STD of FWHM of 8 amplitude distributions were calculated at the coefficients of C from -8×10^{-4} to -5×10^{-4} as shown in Fig. 6(a). The optimized value of $C = -6.24 \times 10^{-4}$ provided the minimum STD, and was used to correct the spectral-resolved interference signals with inexact wavelength distribution. Fig. 6(b) shows the 8 amplitude distributions after signal correction and multiplying R. In order to compare the FWHM obtained with inexact wavelength distribution and signal correction clearly, the values of FWHM were given in Fig. 6(c). According to Fig. 6(c), the FWHM of amplitude distributions obtained with inexact wavelength distribution enlarged with the increase of z, while the FWHM obtained from corrected spectral-resolved interference signals were small and stable at different values of z. The average of FWHM of amplitude distributions obtained with inexact wavelength distribution and signal correction were 22.08 μm and 8.42 μm, respectively. Thus, the axis resolution of the SD-OCT system in relatively deep imaging regions was effectively improved by proposed method. However, the average of FWHM of amplitude distributions obtained from the exact wavelength distribution was 7.33 μm, which was smaller than 8.42 μm obtained with signal correction. The reason is that this method cannot perfectly eliminate the wavelength calibration error of the spectral-resolved interference signals with different Δz by one single coefficient C, which has been explained in the theoretical section.

In order to test the signal correction ability for solving wavelength calibration errors generated by different coefficients in (2), the c_1, c_2 and c_3 were increased 20% from their exact values, respectively. Fig. 7 shows the FWHM obtained with inexact wavelength distribution and signal correction. Table II shows the average value and STD of FWHM of 8 amplitude distributions. The average value and STD of FWHM obtained with corrected

TABLE II
THE AVERAGE VALUE AND STD OF FWHM IN FIG. 7

Coefficient	c_1		c_2		c_3	
	AVERAGE	STD	AVERAGE	STD	AVERAGE	STD
Inexact wavelength (μm)	15.54	6.07	9.34	1.84	14.52	5.06
Signal correction (μm)	6.07	0.39	7.56	0.48	7.83	0.73

spectral-resolved interference signals were smaller than that obtained with inexact wavelength distribution. It indicates that the signal correction is available for different kinds of wavelength calibration errors.

In simulation, the theory to eliminate the nonlinear phase $E(\sigma)$ was proved by the comparison between the calculated value of $C = -1/[4\pi\Delta z(a_1+1)]$ and the optimized C determined by amplitude distribution, and the minor magnitude of nonlinear phase of spectral-resolved interference signal after signal correction. The position error of reflecting surface in measured sample caused by the inexact wavelength distribution was investigated to have a linear relationship with its the actual position and could be eliminated by multiplying the scale factor R. Considering the image quality of all the measurement depths of sample, the optimized coefficient C was obtained by spectral-resolved interference signals with different OPDs, which provided a high resolution. Different kinds of wavelength calibration errors were carried out to verify that the signal correction method has good adaptability.

IV. EXPERIMENT

A commercial SD-OCT was used to verify the effeteness of signal correction method as shown in Fig. 1. The entire OCT system had a superluminescent diode (SLD) light source with the wavelength range of 853 nm-1008 nm. One beam separated by beam-splitter arrived in the reference mirror, which was used to control the OPD. The other beam was focused on the sample after passing the galvanometer scanner and the objective lens. The reflecting beam of the reference mirror and sample were collected by the spectral analyzer system consisting of the grating, lens and camera. A-line signal was acquired at 100kHZ rate with the sampling points of N = 2048. For the cross-sectional imaging, the galvanometer provided a scanning interval of 2 μm and 500 scanning points.

A reflecting mirror was used as the sample to detect the spectral-resolved interference signal. By moving the position of the reference arm, 8 spectral resolved-interference signals with a uniform interval of 300 μm were obtained. The exact and inexact wavelength distributions that were same in Fig. 3, were used to match one group of spectral-resolved interference signals as shown in Fig. 8(a). Fig. 8(b) shows the nonlinear phase component $E(\sigma)$ obtained from the spectral-resolved interference signal with inexact wavelength distribution in Fig. 8(a). After the different values of C were carried out to obtain the STD of FHWMs, the optimized $C = -1.58 \times 10^{-4}$ was acquired and used for signal correction. The FDA method was carried out to calculate Δz as shown in Table III, and the average scale

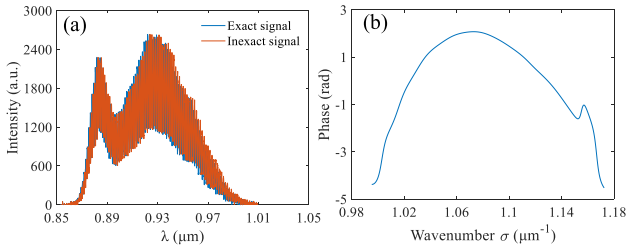

Fig. 8. The spectral-resolved interference signals (a) and obtained nonlinear phase component (b).

TABLE III
THE CALCULATED ΔZ VALUES OBTAINED FROM THE SPECTRAL-RESOLVED INTERFERENCE SIGNALS IN EXPERIMENT

Δz (μm)	300	600	900	1200	1500	1800	2100	2400
Calculated Δz (μm)	301.03	595.56	886.90	1186.23	1484.74	1780.95	2076.84	2371.27
R	0.9966	1.0075	1.0148	1.0116	1.0103	1.0107	1.0112	1.0121

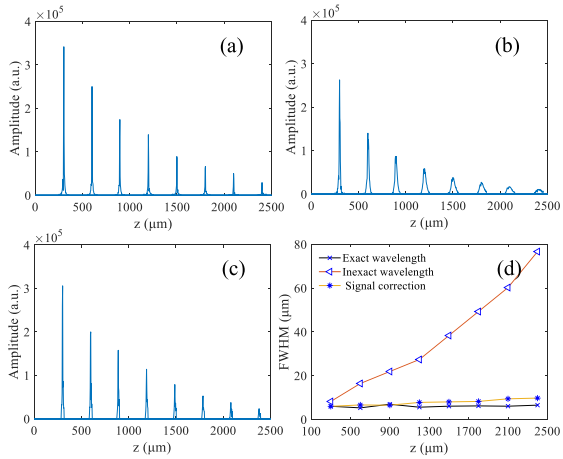

Fig. 9. Amplitude distributions obtained with (a) exact wavelength distribution (b) inexact wavelength distribution and (c) signal correction. (d) FWHM of amplitude distributions in figs. (a)–(c).

factor $R = 1.0094$ between the actual Δz and calculated Δz was also obtained. The average value of R was recorded and used to multiply the position of amplitude distribution after signal correction. Fig. 9(a)–(c) show the amplitude distributions obtained from the spectra-resolved interference signals with exact wavelength distribution, inexact wavelength distribution and signal correction, whose FWHM were given in the Fig. 9(d). The FWHM of amplitude in Fig. 9(a) was stable. The FWHM of amplitude in Fig. 9(b) enlarged with the increase of z. After the signal correction, the FWHM of amplitude in Fig. 9(c) became small and stable that similar with Fig. 9(a). It indicates that the proposed method can significantly improve the axial resolution.

A. Imaging of Tapes

A transparent tape with a thickness of about 1.5 mm was imaged, which had two reflecting surfaces. Same $C = -1.58 \times 10^{-4}$ and nonlinear phase component in Fig. 8(b)

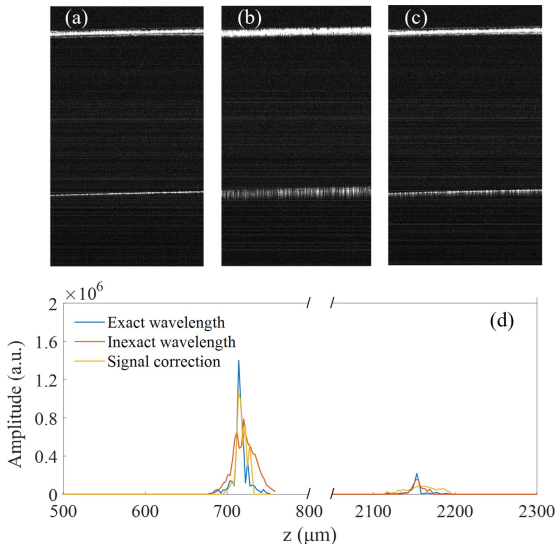

Fig. 10. Images of tape with single layer obtained with (a) exact wavelength distribution (b) inexact wavelength distribution and (c) signal correction. (d) amplitude distributions of one A-scan signal in figs. (a)–(c).

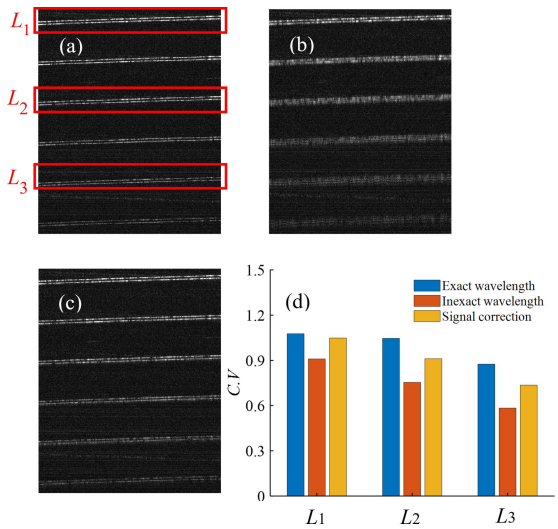

Fig. 11. Cross-sectional images of sample with 6 layers of tape obtained with (a) exact wavelength distribution (b) inexact wavelength distribution and (c) signal correction. (d) histogram of *C.V* values in three districts of the red box.

were carried out for signal correction. Fig. 10(a) and (b) show the images of tape obtained with exact and inexact wavelength distribution shown in Fig. 3(a). After signal correction, Fig. 10(c) shows the image which has a clearer and narrower boundary of front and rear surfaces than that in Fig. 10(b). One A-scan signal was selected to show the amplitude distributions of Fig. 10(a)–(c) in (d). The FWHM of amplitude distributions around z = 720 μm and 2160 μm obtained with exact wavelength distribution are 6.73 μm and 6.26 μm, respectively. The FWHM of amplitude distributions around z = 720 μm and 2160 μm are 33.57 μm and 55.36 μm without signal correction, and decreased to 7.73 μm and 9.99 μm with signal correction.

Fig. 11(a) shows image of sample with 6 layers of tape obtained with the exact wavelength distribution. Performing the

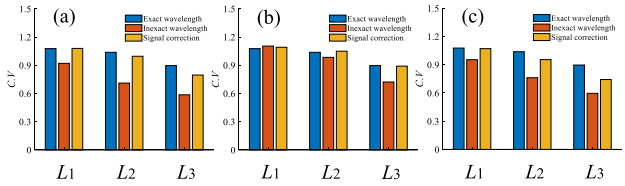

Fig. 12. Histogram of *C.V* obtained with exact coefficients, inexact coefficients of c_1, c_2 and c_3 in (2) and signal correction. (a) c_1 increases 20% from its exact value. (b) c_2 increases 20% from its exact value. (c) c_3 increases 20% from its exact value.

nonlinear phase component in Fig. 8(b) and C $= -1.58 \times 10^{-4}$ on the signal correction for imaging with inexact wavelength distribution, Fig. 11(b) and (c) show the image without and with signal correction. In order to compare the results clearly, the sharpness metric based on variation coefficient was proposed to access the quality [24], which is given by

$$C.V = \frac{\sqrt{\frac{1}{N}\sum_x \sum_y [f(x,y) - \mu]^2}}{\mu} \tag{9}$$

where N is the number of image pixels, $f(x,y)$ is the gray value of pixel, μ is the average gray value of all pixels. The higher the variation coefficient is, the clearer the image will be. Fig. 11(d) shows the *C.V* values obtained with exact wavelength distribution, inexact wavelength distribution and signal correction in L_1, L_2 and L_3 districts of the red box. Compared with the *C.V* values obtained with the inexact wavelength distribution, the *C.V* values increase 15.3%, 17.2%, 26.1% after signal correction in three districts, respectively. It is clear that the *C.V* values increase after signal correction compared with that obtained with inexact wavelength distribution.

Additionally, the c_1, c_2 and c_3 were enlarged 20% from their exact values to act as different kinds of wavelength calibration errors. Fig. 12 shows the sharpness metric of the image obtained with three different inexact wavelength distribution and signal correction. The results indicate that the sharpness metric of image after signal correction has a better performance under the influence of three kinds of wavelength calibration errors except the L_1 district in Fig. 12(b). The possible reason is that the dispersion generated by the tape has an impact on signal correction. This problem is currently being studied and will be solved in the future.

B. *Imaging of Biological Tissue*

To demonstrate that our optimization algorithm is applicable to biological tissues, the sample of chicken breast was imaged by using the nonlinear phase component in Fig. 8(b) and C $= -1.58 \times 10^{-4}$. Fig. 13(a) shows the image of chicken breast tissue obtained with the exact wavelength distribution, and Fig. 13(b) and (c) are the images acquired without and with signal correction, respectively, from which it can be seen that the structure after signal correction is clearer. This improvement can be clearly observed in the lower-right illustration, where the internal lines in the Fig. 13(b) are blurred or missing, and these lines can be better visualized in the Fig. 13(c). The region in the upper half of the lower-right illustration with high intensity

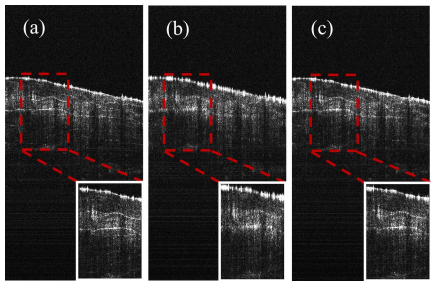

Fig. 13. Cross-sectional images of chicken breast tissue obtained with (a) exact wavelength distribution (b) inexact wavelength distribution and (c) signal correction.

is selected to calculate its *C.V* value. The *C.V* value obtained with the exact wavelength distribution is 2.1953. After signal correction, the *C.V* value of acquired with the inexact wavelength distribution is increased from 1.8272 to 2.0618, which grows 12.8%.

V. Conclusion

This paper presents a method to improve the axial resolution of SD-OCT system in improper wavelength calibration. The nonlinear phase component obtained from spectral-resolved interference signal generated by two reflecting mirrors is used for signal correction by finding an optimized coefficient through the algorithm. The optimized coefficient and the nonlinear phase component are recorded and used to correct spectral-resolved interference signals produced by any other samples. In the measurement of one tape with a thickness of about 1.5 mm, the FWHM of amplitude distributions of one selected A-scan signal decrease to 7.73 μm and 9.99 μm from 33.57 μm and 55.36 μm. The sharpness metric of image of sample made of 6 layers of tapes and a small chicken breast grow larger than 12.8% after signal correction. This method provides a new approach to solve the wavelength calibration error in SD-OCT. Since the sample-dependent dispersion also brings the nonlinear phase component for the spectral-resolved interference signal that is similar with the inaccurate wavelength calibration, the investigation will be carried out to eliminate the error caused by the sample-dependent dispersion and inaccurate wavelength calibration together in the future.

Disclosures

The authors declare that there are no conflicts of interest related to this article.

Data Availability

Data will be made available on request.

References

[1] D. Huang et al., "Optical coherence tomography," *Science*, vol. 254, no. 5035, pp. 1178–1181, 1991, doi: 10.1126/science.1957169.

[2] M. Wojtkowski, R. Leitgeb, A. Kowalczyk, and T. Bajraszewski, "In vivo human retinal imaging by Fourier domain optical coherence tomography," *J. Biomed. Opt.*, vol. 7, no. 3, pp. 457–463, 2002, doi: 10.1117/1.1482379.

[3] G. Hausler and M. W. Lindner, "'Coherence Radar' and 'Spectral Radar'—New tools for dermatological diagnosis," *Proc. SPIE*, vol. 3, no. 1, pp. 21–31, 1998, doi: 10.1117/1.429899.

[4] R. Leitgeb, C. K. Hitzenberger, and A. F. Fercher, "Performance of Fourier domain vs. time domain optical coherence tomography," *Opt. Exp.*, vol. 11, no. 8, pp. 889–894, 2003, doi: 10.1364/oe.11.000889.

[5] J. F. de Boer, B. Cense, B. H. Park, M. C. Pierce, G. J. Tearney, and B. E. Bouma, "Improved signal-to-noise ratio in spectral-domain compared with time-domain optical coherence tomography," *Opt. Lett.*, vol. 28, no. 21, pp. 2067–2069, 2003, doi: 10.1364/ol.28.002067.

[6] M. Wojtkowski, V. Srinivasan, T. Ko, J. Fujimoto, A. Kowalczyk, and J. Duker, "Ultrahigh resolution, high-speed, Fourier domain optical coherence tomography and methods for dispersion compensation," *Opt. Exp.*, vol. 12, no. 11, pp. 2404–2242, 2004, doi: 10.1364/opex.12.002404.

[7] C. H. Tseng, J. F. Ford, C. K. Mann, and T. J. Vickers, "Wavelength calibration of a multichannel spectrometer," *Appl. Spectrosc.*, vol. 47, no. 11, pp. 1808–1813, 1993, doi: 10.1366/0003702934065948.

[8] J. Cho, P. J. Gemperline, and D. Walker, "Wavelength calibration method for a CCD detector and multichannel fiber-optic probes," *Appl. Spectrosc.*, vol. 49, no. 12, pp. 1841–1845, 1995, doi: 10.1366/0003702953966055.

[9] X. W. Du, C. Y. Li, Z. Xu, and Q. P. Wang, "Accurate wavelength calibration method for Flat-Field grating spectrometers," *Appl. Spectrosc.*, vol. 65, no. 9, pp. 1083–1086, 2011, doi: 10.1366/11-06280.

[10] P. Martinsen, B. Jordan, A. McGlone, P. Gaastra, and T. Laurie, "Accurate and precise wavelength calibration for wide bandwidth array spectrometers," *Appl. Spectrosc.*, vol. 62, no. 9, pp. 1008–1012, 2008, doi: 10.1366/000370208785793399.

[11] Z. Wang, Z. Yuan, H. Wang, and Y. Pan, "Increasing the imaging depth of spectral-domain OCT by using interpixel shift technique," *Opt. Exp.*, vol. 14, no. 16, pp. 7014–7023, 2006, doi: 10.1364/oe.14.007014.

[12] C. Ding, P. Bu, X. Z. Wang, and O. Sasaki, "A new spectral calibration method for Fourier domain optical coherence tomography," *Optik*, vol. 121, no. 11, pp. 965–970, 2010, doi: 10.1016/j.ijleo.2008.12.016.

[13] M. Mujat, B. H. Park, B. Cense, T. C. Chen, and J. F. de Boer, "Autocalibration of spectral-domain optical coherence tomography spectrometers for in vivo quantitative retinal nerve fiber layer birefringence determination," *Proc. SPIE*, vol. 12, no. 4, 2007, Art. no. 041205, doi: 10.1117/1.2764460.

[14] X. Liu, M. Balicki, R. H. Taylor, and J. U. Kang, "Towards automatic calibration of Fourier-domain OCT for robot-assisted vitreoretinal surgery," *Opt. Exp.*, vol. 18, no. 23, pp. 24331–24343, 2010, doi: 10.1364/oe.18.024331.

[15] Y. Chen et al., "Automatic spectral calibration for polarization sensitive optical coherence tomography," *Opt. Exp.*, vol. 25, no. 20, pp. 23605–23618, 2017, doi: 10.1364/oe.25.023605.

[16] S. Moon, Y. Qu, and Z. Chen, "Characterization of spectral-domain OCT with autocorrelation interference response for axial resolution performance," *Opt. Exp.*, vol. 26, no. 6, pp. 7253–7269, 2018, doi: 10.1364/oe.26.007253.

[17] R. A. Leitgeb et al., "Ultrahigh resolution Fourier domain optical coherence tomography," *Opt. Exp.*, vol. 12, no. 10, pp. 2156–2165, 2004, doi: 10.1364/OPEX.12.002156.

[18] Y. Yasuno et al., "Three-dimensional and high-speed swept-source optical coherence tomography for in vivo investigation of human anterior eye segments," *Opt. Exp.*, vol. 13, no. 26, pp. 10652–10664, 2005, doi: 10.1364/opex.13.010652.

[19] K. Wang and Z. Ding, "Spectral calibration in spectral domain optical coherence tomography," *Chin. Opt. Lett.*, vol. 6, no. 12, pp. 902–904, 2008.

[20] R. de la Fuente, "White light spectral interferometry as a spectrometer calibration tool," *Appl. Spectrosc.*, vol. 68, no. 5, pp. 525–530, 2014, doi: 10.1366/13-07315.

[21] Y. R. Chen et al., "Densely folded spectral images of a CCD spectrometer working in the full 200–1000 nm wavelength range with high resolution," *Opt. Exp.*, vol. 13, no. 25, pp. 10049–10054, 2005, doi: 10.1364/opex.13.010049.

[22] X. Attendu, R. M. Ruis, C. Boudoux, T. G. van Leeuwen, and D. J. Faber, "Simple and robust calibration procedure for k-linearization and dispersion compensation in optical coherence tomography," *Proc. SPIE*, vol. 24, no. 5, 2019, Art. no. 056001, doi: 10.1117/1.jbo.24.5.056001.

[23] P. de Groot and L. Deck, "Surface profiling by analysis of white-light interferograms in the spatial frequency domain," *J. Modern Opt.*, vol. 42, no. 2, pp. 389–401, 1995, doi: 10.1080/09500349514550341.

[24] L. H. Pan et al., "Depth-dependent dispersion compensation for full-depth OCT image," *Opt. Exp.*, vol. 25, no. 9, pp. 10345–10354, 2017, doi: 10.1364/oe.25.010345.